J Appl Electrochem (2009) 39:1033–1038
DOI 10.1007/s10800-008-9751-8

ORIGINAL PAPER

Morphology-dependent electrochemical supercapacitive characteristics of nanostructured manganese dioxide

Guo-Qing Zhang · Sheng-Tao Zhang

Received: 11 July 2008 / Accepted: 5 December 2008 / Published online: 20 December 2008

Abstract The dependence on morphology of the supercapacitive characteristics of manganese dioxide nanospheres (NSs) and nanorods (NRs) was investigated by X-ray diffraction (XRD), scanning electron microscopy (SEM), and a series of electrochemical techniques. Because the nanosized pores in MnO_2 NSs resulted in high surface area, MnO_2 electrodes made of NSs had higher specific capacitance (SC) than those made of NRs at current densities less than 2.0 A g^{-1}. However, at current densities over 2.0 A g^{-1}, the power density of MnO_2 electrodes composed of NRs was better than that of NSs. The high surface area and nanosized pores in MnO_2 NSs increase the number of redox active sites, which leads to high specific capacitance. On the other hand, the small pore size in MnO_2 NSs restricts the rates of charge and discharge, thus limiting their power density.

Keywords Active site · Electrochemical supercapacitors · Manganese dioxide · Nanostructure

1 Introduction

Electrochemical supercapacitors [1–3], which are intermediate between conventional dielectric capacitors and batteries in terms of energy and power density, have attracted enormous attention in recent years [4, 5]. The main objective of many studies was to increase the energy density of supercapacitors. The energy (E, in joules) stored in a supercapacitor with capacitance C (in farads) and working voltage V is defined by the equation $E = 1/2CV^2$. This formula suggests two ways to increase the stored energy. One is to increase the specific capacitance. The other is to increase the voltage between the positive and negative electrodes. Capacitance can be increased by using electrode materials with high specific capacitance. The materials studied for supercapacitors have been mainly of three types: carbon/carbon [6], metal oxides [7–9], and electrically conducting polymers [10]. Carbon materials (activated carbon black, carbon aerogel, and carbon nanotubes) are used in electric double-layer capacitors (EDLC), which are based on electrical charge separation at the interface between electrode and electrolyte. Metal oxides and conducting polymers are generally used in pseudocapacitors, whose activity results from electrical charge transport in redox reactions.

Electric double-layer capacitance is present at all electrode/electrolyte interfaces but traditionally has been studied only for supercapacitors based on carbon materials. According to the capacitance formula $C_{dl} = \varepsilon A/4\pi d$, increasing the surface area of carbon can improve its capacitance; high surface-area porous carbon is the most suitable form. However, the availability of surface area is a crucial question for porous carbon. Recently, Celine et al. [11] investigated the relation between ion size and pore size for double-layer capacitors. They proposed a general principle for selecting a porous electrode/electrolyte system: the pore size of electrode material providing the maximum double-layer capacitance is very close to the size

G.-Q. Zhang · S.-T. Zhang
College of Chemistry and Chemical Engineering, Chongqing University, Chongqing 400030, People's Republic of China

G.-Q. Zhang (✉)
Department of Chemistry and Environment Science, Yangtze Normal University, Chongqing 408100, People's Republic of China
e-mail: yzhanggq@163.com

of the ions in the electrolyte. Both larger and smaller pores lead to significant drops in capacitance.

Metal oxides, such as RuO_2 [12–15], MnO_2 [16–18], NiO [19], etc., are generally considered pseudocapacitors, because their charge storage depends on chemical redox reactions at the interface between electrode and electrolyte. Among these metal oxides, manganese dioxide has been widely studied for electrochemical supercapacitors because it is cost-effective and non-polluting. In particular, various nanostructured manganese dioxides now available have attracted enormous attention. Manganese dioxide can be prepared with two different nanostructures: nanospheres (NSs) and nanorods (NRs). However, few reports are available on the relationship between the morphology and the supercapacitive behavior of manganese dioxide. To fill this gap, we have studied the electrochemical characteristics of MnO_2 nanospheres and nanorods. On the basis of our experimental observations, we discuss the relationship between morphology and supercapacitance in these materials.

2 Experimental

2.1 Synthesis of nanostructured MnO_2

Nanospheres of MnO_2 were prepared according to [20], by the reaction of a dilute $MnSO_4$ solution with permanganic acid at room temperature. Fresh permanganic acid must be prepared just before use by treating a permanganate salt with hydrochloric acid. To prevent undesirable byproducts, we used silver permanganate purchased from Aldrich with no further purification. Silver chloride is insoluble in water, which prevents metal ions from entering the synthetic structure. The preparation was as follows: 5 mL of 0.5 M HCL was added dropwise to 100 mL of 0.025 M $AgMnO_4$ solution. After vigorous stirring at room temperature for 10 min, the mixture was centrifuged and decanted. The resulting pink solution was added dropwise to 300 mL of 0.02 M $MnSO_4$ with rapidly stirring over 12 h at room temperature. The slurry obtained was filtered and washed with distilled water at least four times and then dried in air at 120 °C for 12 h. The final product was a black powder.

Nanorods of MnO_2 were obtained by hydrothermal treatment of the nanospheres. In a typical synthesis, 1 g of the nanospheres was added to 50 ml of distilled water in a Teflon-lined 80-ml-capacity autoclave. After the suspension was stirred for 1 min with a stainless-steel muddler, the autoclave was sealed and heated at 150 °C for 24 h. After cooling to room temperature, the product was collected by filtration, washed with distilled water, and dried at 40 °C.

2.2 Physical measurements

X-ray diffraction (XRD; MAC, M18XCE, Japan; with Cu K_α radiation; $\lambda = 0.15418$ nm) was used to characterize the crystalline structure of the MnO_2 preparations. Their morphology was observed with a scanning electron microscope (SEM; JEOL-600, Japan).

2.3 Electrochemical measurements

The MnO_2 electrodes were prepared as follows. A mixture containing 80 wt% MnO_2, 15 wt% acetylene black (AB) and 5 wt% polytetrafluoroethylene (PTFE) was well mixed, and then pressed (1.2×10^7 Pa) onto a nickel grid (0.2 cm^2) that served as a current collector. The typical mass load of MnO_2 was 4 mg. All electrochemical measurements were conducted in 1 M Na_2SO_4 solution at 25 °C with a beaker-type electrochemical cell. It was equipped with a prepared MnO_2 electrode as the working electrode, a platinum foil counter electrode, and a saturated calomel (SCE) reference electrode. Cyclic voltammetry (CV) and galvanostatic charge-discharge of the electrode were carried out between 0 and 1.0 V (vs. SCE) using a CHI760C electrochemical workstation.

3 Results and discussion

3.1 Structure and morphology of MnO_2

The XRD patterns of the synthesized materials are shown in Fig. 1. As can been seen, the patterns for the two MnO_2 preparations are very similar, indicating that the crystalline phases of the two products were almost the same. The patterns show well-defined reflections, which signify pure crystalline phase structures. The characteristic diffraction peaks were assigned as 22.5° (120), 37.1° (131), 42.5°

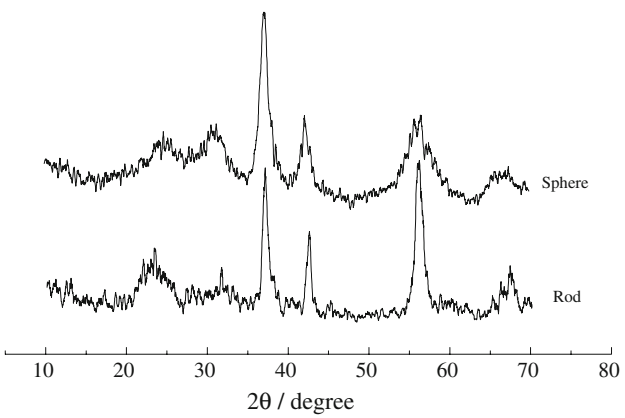

Fig. 1 XRD patterns of nanospheres and nanorods

(300), 56.4° (160), and 67.2° (003). Structural analysis further revealed that the MnO_2 samples were all composed of typical hexagonal γ-MnO_2, which has the lattice parameters $a = 6.36$ Å, $b = 10.15$ Å, $c = 4.09$ Å. However, the intensities of some diffraction peaks were different, showing that the samples had different morphologies and sizes.

To illustrate the morphologies of the synthesized materials, SEM images are presented in Fig. 2. The morphologies of these two MnO_2 preparations revealed distinct nanostructural features. As shown in Fig. 2(a, b), the NS material tends to form spherical particles with many flakes arranged uniformly to form the surface of each nanosphere. The average nanosphere size is about 1 μm. At a magnification of 100,000×, the SEM image (Fig. 2b) shows the existence of a bird's nest morphology and the nanostructured flakes. The nanosphere is actually made up of networks of solid flakes and pores with a size of 20–50 nm. Hollow [20] nanospherical manganese dioxide exhibits a large surface area and has numerous nano-pores. These hollow nanostructured particles result in materials with a high density of active sites for promoting fluid/solid reactions, and provide a relatively easy path for percolation of the reactive fluid through the material. Therefore, this type of MnO_2 should be an outstanding material for supercapacitor electrodes.

After hydrothermal treatment of the nanospheres, rod-like MnO_2 (shown in Fig. 2(c, d)) was formed with an average length of several μm and an average diameter of about 400 nm. Combining the XRD patterns and SEM images of these two MnO_2 preparations, we can conclude that the hydrothermal treatment changed the morphology but not the crystalline phase of the material.

3.2 Electrochemical supercapacitive characteristics of MnO_2 electrode

Cyclic Voltammetry (CV) is a suitable experimental technique for evaluating the electrochemical capacitive properties of active materials. Therefore, we used cyclic voltammetry in the potential range between 0 and 1.0 V to measure the electrochemical properties of the MnO_2 electrodes. Figure 3 show typical voltammograms for the MnO_2 preparations in 1 M Na_2SO_4 electrolyte recorded at different scan rates. The voltammograms do not exhibit any sharp redox peaks in the potential range studied. The rectangular voltammograms exhibit mirror image cathodic and anodic parts, suggesting an ideal capacitive behavior of

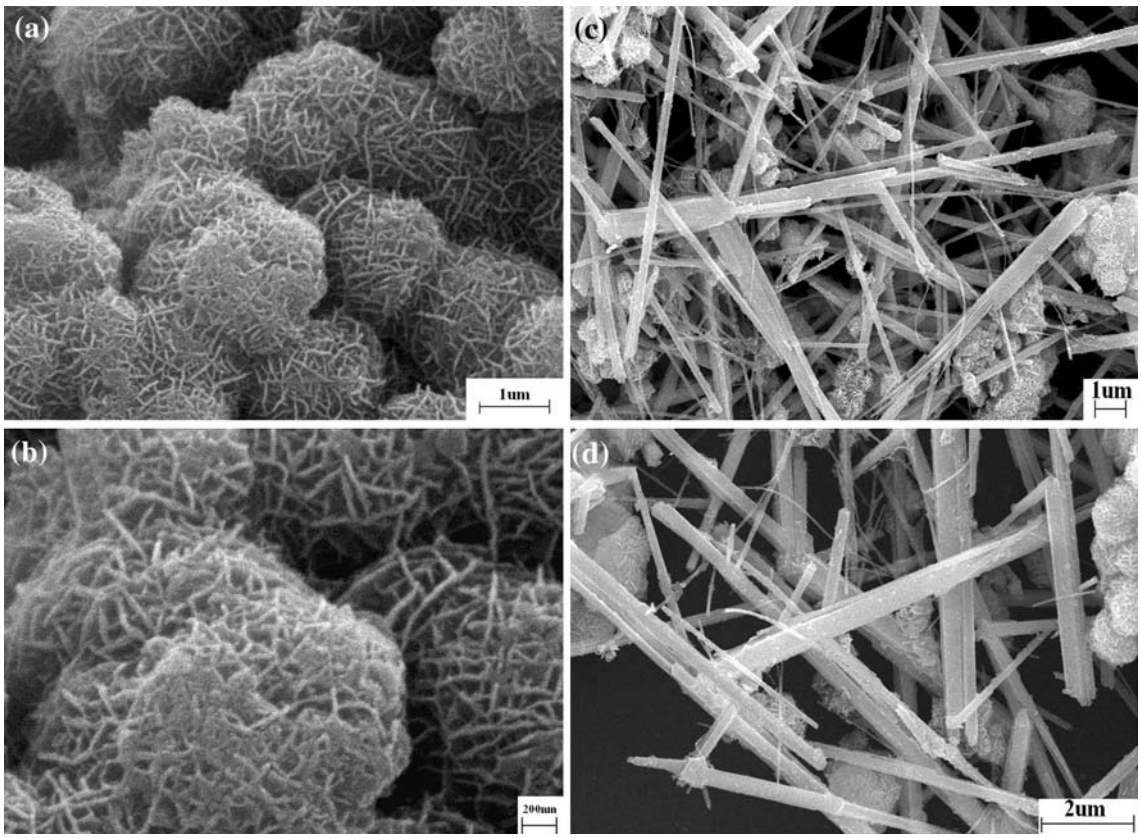

Fig. 2 SEM images of MnO_2 (**a**, **b**) nanospheres (**c**, **d**) nanorods

the materials. The variation of voltammetric cathodic current density with sweep rate is shown in Fig. 3b. The cathodic currents in MnO_2 nanorod electrodes at various scan rates are clearly higher than those of MnO_2 nanospheres (Fig. 3b). The change in morphology from NS to NR accelerates the redox reaction rate, allowing an increase in current density. Because capacitance is proportional to stored charge, it can be calculated using the relation

$$C = C_0 e^{-aeV/K_B T}$$

where C is capacitance, C_0 is intrinsic capacitance that depends on the position of the conduction band of MnO_2, and V is the potential. The MnO_2 NR electrode showed high cathodic and anodic charges due to the rod-like shape of the NRs, indicating that the redox reactions (related to pseudocapacitance) were more extensive in the MnO_2 NR electrode than in the NS electrode.

As Fig. 3a shows, the voltammetric currents for the two nanostructured MnO_2 electrodes changed very little over 200 cycles, indicating a good cycle stability of both MnO_2 forms.

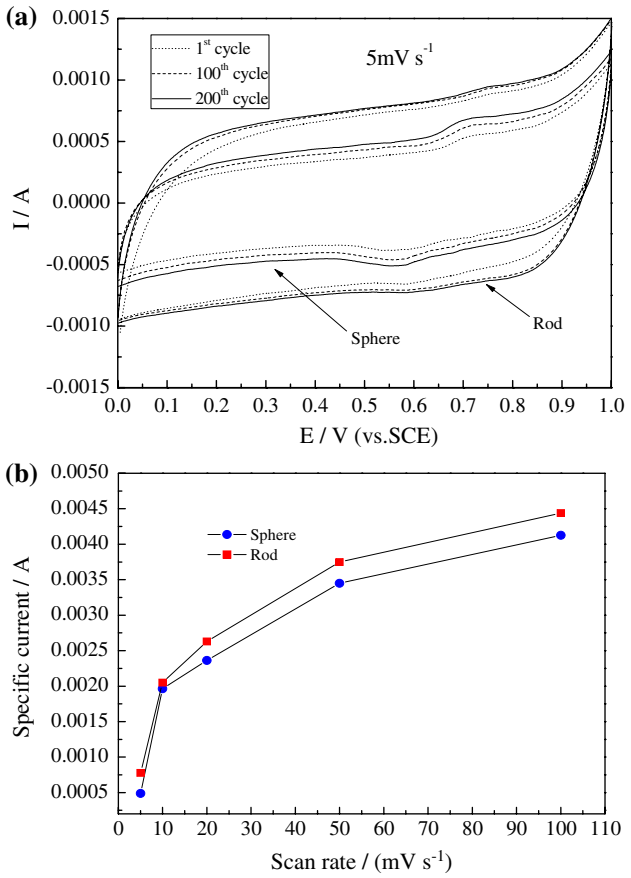

Fig. 3 **a** Cyclic voltammograms. **b** Specific current against scan rate

To further investigate the supercapacitive performance of the MnO_2 electrodes, we measured their galvanostatic charge/discharge curves over the range of 0–1.0 V. The curves presented in Fig. 4a show two distinct regions: first, a linear region (0.0–0.1 V) due to electrochemical double-layer capacitance, and second, a convex region (0.1–1.0 V) caused by pseudocapacitance. The MnO_2 NS electrode exhibited a high specific capacitance (SC) of 50 F g^{-1} at the low discharge current density of 0.5 A g^{-1}. Nanospherical MnO_2, because of its large surface area, can provide many active sites for redox reactions and large EDLC, resulting in high SC at discharge current densities up to 2.0 A g^{-1}. The calculated SC value for the NS electrode as displayed in Fig. 4b is about 30% higher than that of the NR electrode at that current density. This result disagrees with that of CV. However, the SC of the NS electrode decreased sharply when the discharge current density increased from 0.5 to 2.5 A g^{-1}. The decrease in the SC of the NR electrode was small, demonstrating the high power characteristic of MnO_2 NR electrodes. Apparently, at discharge current densities above 2.0 A g^{-1}, diffusion of the electrolyte through the narrow pores in the nanospheres becomes rate-limiting. Consequently, the available surface area in NS electrodes decreases, which results in low electric double-layer capacitance (EDLC), and the SC of NS electrodes decrease accordingly. The change in the available redox reaction active sites of rod-like MnO_2 with current density is significantly less than that of nanospherical MnO_2, indicating a fast redox reaction on the NR electrode. To illustrate this difference, we calculated the available redox reaction active sites per mole (Z) from the specific capacitance according to the following relation [21]

$$Z = C(\Delta V)M/F$$

where ΔV is the potential window, M is the molecular weight of MnO_2, F is the Faraday constant, and C is the SC. A plot of the calculated active sites of nanostructured MnO_2 against the discharge current density, as shown in Fig. 4c, suggests that the change in morphology from NS to NR decreased the number of redox reaction sites from 0.045 to 0.03 at a discharge current density of 0.5 A g^{-1}. At a discharge current density of 2.5 A g^{-1}, the number of available redox reaction sites changed from 0.0135 to 0.0145. In Fig. 4b, the slope of the linear fit to the curve (specific capacitance against discharge current) for the NS electrode is steeper than for the NR electrode, indicating a greater increase in charge transfer resistance in the NS electrode than in the NR electrode. The small pore size (20–50 nm) in nanospherical MnO_2 restrains the movement of the reaction ions (electrolyte ions) into the material, resulting in high charge transfer resistance for redox reactions that take place inside the nanoparticles.

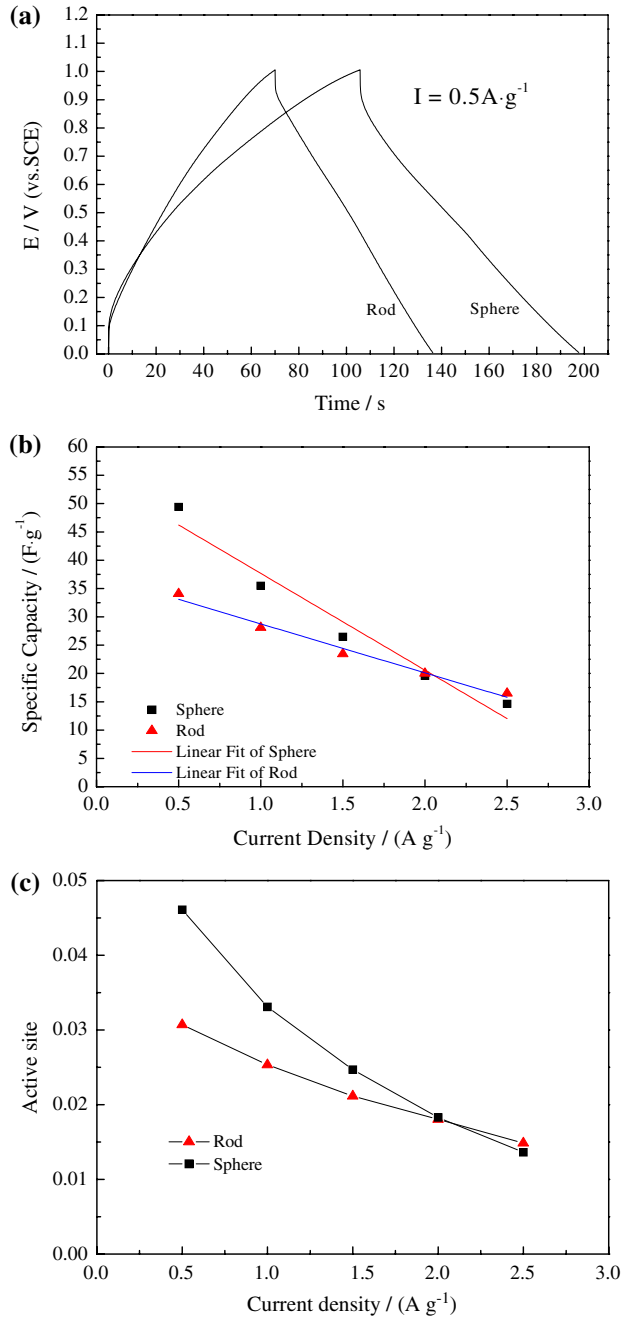

Fig. 4 **a** Charge/discharge curves, **b** Specific capacitance, and **c** Reaction active sites of MnO_2 against discharge current density. The mass of MnO_2 was 4 mg

To verify this interpretation, we performed electrochemical impedance spectroscopy over the frequency range of 10^5–10^{-2} Hz. The plots shown in Fig. 5 consist of a semicircle and a spike. The semicircle in the higher frequency region is associated with the charge transfer processes occurring at the electrode/electrolyte interface, and the spike at lower frequencies region is associated with the diffusion of electrolyte ions into MnO_2 particles. Judging from the semicircle in the higher frequency region,

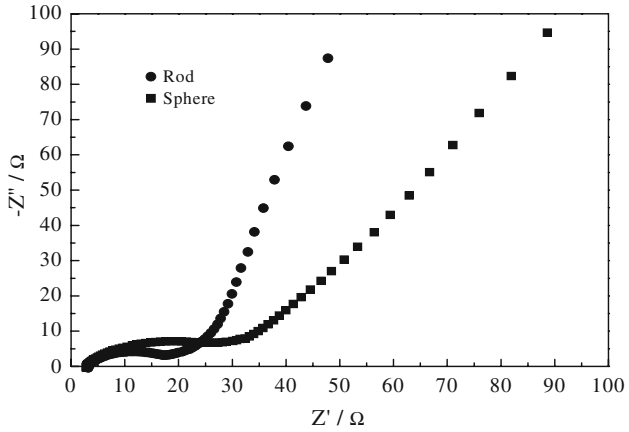

Fig. 5 Electrochemical impedance spectra of the MnO_2 electrodes. The imaginary part (Z'') of the complex impedance is plotted against the real part (Z'). Larger values of Z' correspond to lower frequencies

the charge transfer resistance of NRs is less than that of NSs, which again indicates the speed of the redox reactions in NR electrodes. This observation further confirms that MnO_2 NR electrodes have high power density.

4 Conclusions

MnO_2 nanoparticles with different morphologies, NSs and NRs, were prepared by chemical deposition and simple hydrothermal methods. Their supercapacitive characteristics were investigated with electrochemical techniques. The MnO_2 nanospheres have higher specific capacitance at low current density (less than 2.0 A g^{-1}), but at current densities over 2.0 A g^{-1}, NRs of MnO_2 have better power characteristics. These experimental observations can be explained by differences in surface area, pore size and redox reaction active sites, leading to changes in EDLC and faradic pseudocapacitance. This work provides general guidance for MnO_2 and other nanocrystals with controllable sizes and shapes for different supercapacitor applications.

Acknowledgments This work was supported by Yangtze Normal University Research Start-up Foundation and Science and Technology Research Project of Chongqing Education Board (KJ081304).

References

1. Winter M, Brodd RJ (2004) Chem Rev 104:4245
2. Burke A (2000) J Power Sources 91:37
3. Conway BE (1999) Electrochemical supercapacitors scientific fundamentals and technological applications. Kluwer Academic/Plenum Press, New York
4. Sarangapani S, Tilak BV, Chen CP (1996) J Electrochem Soc 143:3791
5. Reddy RN, Reddy RG (2004) J Power Sources 132:315

6. Nakagava H, Shudo A, Miura K (2000) J Electrochem Soc 147:38
7. Novak P, Müller K, Santanam KSV, Hass O (1997) Chem Rev 97:207
8. Jeong YU, Manthiram A (2001) J Electrochem Soc 148:A189
9. Cao L, Kong LB, Liang YY, Li HL (2004) Chem Commun 14:1646
10. Zhou YK, He BL, Zhou WJ, Li HL (2004) J Electrochem Soc 151:A1052
11. Celine L, Cristelle P, John C, Pierre-Louis T, Yury G, Patrice S (2008) J Am Chem Soc 130:2730
12. Ardizzone S, Fregonara G, Trasatti S (1990) Electrochimica Acta 35:263
13. Kim H, Popov BN (2002) J Power Sources 104:52
14. Chang KH, Hu CC (2004) Electrochem Solid-State Lett 7:A466
15. Soudan P, Gaudet J, Guay D, Bélanger D, Schulz R (2002) Chem Mater 14:1210
16. Lee HY, Goodenough JB (1999) J Solid State Chem 144:220
17. Pang SC, Anderson MA, Chapman TW (2000) J Electrochem Soc 147:444
18. Toupin M, Brousse T, Bélanger D (2004) Chem Mater 16:3184
19. Zhao DD, Bao SJ, Zhou WJ, Li HL (2007) Electrochem Commun 9:869
20. Yuan JK, Laubernds K, Zhang QH, Suib LS (2003) J Am Chem Soc 125:4966
21. Srinivasan V, Weidner JW (2000) J Electrochem Soc 147:880